Stabilization and Early Degradation of UV-Irradiated Heterophasic Propylene−Ethylene Copolymers Based on ESR, ESR Imaging, UV−Vis, and DSC: Effect of Ethylene Content and UV Wavelength

Krzysztof Kruczala,† Wasim Aris, and Shulamith Schlick*

Department of Chemistry and Biochemistry, University of Detroit Mercy, Detroit, Michigan 48221

Received February 1, 2005; Revised Manuscript Received June 7, 2005

ABSTRACT: Heterophasic propylene−ethylene copolymers (HPEC) containing 1 wt % bis(2,2,6,6-tetramethyl-4-piperidinyl) sebacate (Tinuvin 770) as a hindered amine stabilizer (HAS) were aged by exposure of ≈3 mm thick plaques to UVA and UVB sources in weathering chambers at 318 K. Two types of copolymers, HPEC1 and HPEC2, were examined, which contained 25 and 10 wt % ethylene (E), respectively, as ethylene/propylene rubber (EPR). Spatial and temporal effects of the aging process were studied by electron spin resonance (ESR) and ESR imaging (ESRI) of HAS-derived nitroxide radicals (HAS-NO), by comparison of thermal transitions in original and aged samples using DSC, and by measuring the UV−vis absorption of HPEC films as a function of their thickness. ESR spectra indicated the presence of nitroxide radicals in two amorphous sites, fast (F) and slow (S). The spatial distribution of HAS-NO was obtained by 1D ESRI. Nondestructive ("virtual") slicing of the 2D spectral−spatial ESR images resulted in a series of ESR spectra that reflected the variation of the F/S intensity ratio with sample depth. HAS-NO was detected on the nonirradiated side due to the small, but not negligible, intensity of UV light transmitted through the plaque; on this side the nitroxide concentration remains high because it is not consumed in stabilization processes, as the local rate of degradation is low. Both ESRI and DSC experiments indicated a higher degradation rate in HPEC2, which contained more polypropylene (PP), 90 wt %; in these samples the degradation was accompanied by an increase in the extreme separation in the ESR spectra, indicating slower dynamics as a result of the increased degree of crystallinity. The degradation was also more advanced in samples exposed to UVB radiation compared to UVA due to the higher UV absorption coefficient in the shorter λ range. The different effect of EPR content in thermal and UV aging of HPEC samples was discussed.

Introduction

The spatial variation of degradation rates (within sample depth) can be deduced by electron spin resonance imaging (ESRI) in polymers containing hindered amine stabilizers (HAS); this approach was originally suggested by Ohno, who presented 2D spectral−spatial ESRI images of radicals in polypropylene (PP) containing two different stabilizers, but no detailed analysis.[1] The method is based on the facile formation of stable nitroxide radicals derived from HAS (termed HAS-NO) during UV irradiation or thermal treatment and on encoding spatial information in the ESR spectra via magnetic field gradients. The chemistry of hindered amines has been widely documented: Transformation of the amines to nitroxides occurs by reaction with peroxy radicals ROO•; the efficient stabilization mechanism is based on scavenging of polymer-derived radicals by the nitroxides, leading to the formation of diamagnetic species.[2,3]

Lucarini et al. have determined by 1D ESRI the distribution of the nitroxide radicals in UV-irradiated PP containing a hindered amine stabilizer.[4,5] The spatial variation of nitroxide intensity in samples irradiated for long times was explained by the diffusion-limited oxidation (DLO) concept:[6−8] The extent of degradation depends on the transport of oxygen through the sample depth. When the consumption of oxygen in oxidation processes is lower than or comparable to the amount of oxygen available by diffusion, degradation can occur through the entire sample. If, however, the rate of oxygen consumption is higher that its supply rate, only layers in contact with air are degraded, and the sample interior is not affected; this is the DLO regime. The DLO regime and high oxidation rates lead to narrow penetration depth of oxygen.[9f]

In our laboratory we have developed 1D and 2D spectral−spatial ESRI for the study of heterophasic systems such as poly(acrylonitrile−butadiene−styrene) (ABS)[9] and propylene−ethylene copolymers (HPEC).[10] In these systems the HAS-derived nitroxides perform a triple role. First, they provide the contrast needed in the imaging experiments. Second, they enable the visualization of polymer morphology, based on the detection of two dynamically different components detected in the ESR spectra of the nitroxides; in ABS for instance, the two sites, fast (F) and slow (S), have been assigned to location of nitroxides in butadiene-rich and styrene−acrylonitrile (SAN)-rich domains, respectively. Third, the spatial variation of the ESR spectra of nitroxides (in terms of intensity and line shapes) with treatment time, t, provides detailed information on the extent of degradation in the different microdomains. These experiments made possible the determination not only of the concentration profiles of the nitroxides but also of spectral profiling: the variation of ESR spectra with sample depth.

Conclusions from the 1D and 2D ESRI experiments have been further confirmed by ATR-FTIR, which measured the variation of the carbonyl signal at ≈1730 cm^{-1} and, in ABS, of the butadiene signal at 966 cm^{-1}, as a function of treatment time.[9−11] Previous studies have emphasized that the advantage of ESRI compared to FTIR is the ability to determine mechanistic details

† On leave from the Faculty of Chemistry, Jagiellonian University, Cracow, Poland.

* Corresponding author. E-mail: schlicks@udmercy.edu.

10.1021/ma0502194 CCC: $30.25
Published on Web 07/14/2005

on the early stages of degradation;[9d] this advantage is a direct result of the exceptional sensitivity of ESR methods for the detection of radical species. Additional details on the thermal transitions and nitroxide dynamics were obtained by ESR of polymers containing nitroxide spin probes as dopants.[12]

Heterophasic propylene−ethylene copolymers (HPEC), known commercially as impact polypropylene copolymers (IPC), consist of crystalline polypropylene modified by an elastomeric component, typically ethylene−propylene rubber (EPR). The polymers are usually prepared by polymerization of propylene in the presence of catalysts, followed by sequential polymerization of a propylene−ethylene mixture with the same catalysts.[13] The application of ESR spectroscopy, ESRI, and FTIR to the study of degradation in HPEC samples thermally treated at 393 and 433 K has been reported.[10] Both ESRI and FTIR experiments suggested a faster degradation rate in HPEC1 containing the higher amount of the EPR component (25 wt % E) compared to HPEC2 (10 wt % E); moreover, a higher amount of Tinuvin 770 in the polymers led to *less* efficient stabilization. FTIR spectra indicated increased ordering of polypropylene segments in HPEC during aging at 433 K. The study of thermal aging has shown that a major advantage of the ESRI method is the ability to reveal degradation and stabilization within the sample depth in a nondestructive way. In addition, in heterophasic polymers such as HPEC and ABS systems, 1D and 2D spectral−spatial ESRI allowed separate visualization of degradation processes in various *amorphous* phases,[9,10] including the rigid amorphous phase (RAP) detected by ESR in the case of HPEC.[10a] The RAP is the part of the amorphous phase that is modified by the proximity to the crystalline phase and is the interphase characterized by partial order in the three-phase model for semicrystalline polymers.[14−17] Experimental studies have explored the mechanical properties of the interphase, differences in specific heat, small-angle X-ray scattering (SAXS), NMR, FTIR, and Raman spectra. The picture that emerged from these studies is that the boundary between crystalline and totally disordered domains is not sharp. In some systems a broadening of the glass transition and an increase in T_g with increasing degree of crystallinity were observed. A decrease of the change in specific heat, ΔC_p, beyond that expected for the amount of polymer that has crystallized, has also been detected in some cases, and has been taken as an indicator of some rigidity in the amorphous phase. These phenomena have been rationalized by assuming the presence of a *rigid amorphous phase*.

The photodegradation and stabilization of heterophasic propylene−ethylene copolymers containing 15 wt % ethylene as EPR has been studied by Delprat et al. using medium-pressure mercury lamps as the irradiation source ($\lambda > 300$ nm).[18] The polymers were studied as 100 μm thick films and 3 mm thick plaques, with FTIR and photoacustic spectroscopy (PAS) as the main methods of study. Some experiments were also performed on samples stabilized by two types of hindered amine light stabilizers, HALS-1 and HALS-2.[19] The major conclusion was that the degradation of the copolymers is dominated by the susceptibility of the propylene component to both thermal degradation and photodegradation; as such, interpretation of the results in the heterophasic copolymers benefits from numerous and detailed degradation studies of PP, which have been performed using a wide variety of investigation methods.[20−25] The copolymer behavior is, however, more complicated compared to pure PP: the presence of the EPR component leads to a complex phase structure that includes not only crystalline and amorphous PP domains but also the rigid amorphous phase and the amorphous rubber phases.[10,25] The EPR phase also increases the rate of oxygen diffusion through the copolymer, and therefore composition is a parameter that is expected to play a major role in the degradation behavior but has not been investigated yet.

Chart 1. Hindered Amine Stabilizer (HAS) Tinuvin 770

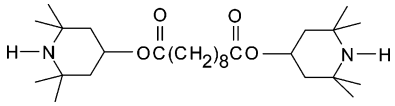

We present a study of photodegradation in HPEC systems containing a hindered amine stabilizer (Tinuvin 770); aging was performed by exposure of ≈3 mm thick plaques to UVA and UVB sources in weathering chambers at 318 K. As in thermal aging, two types of HPEC were examined, containing 25 and 10% ethylene (E) as ethylene/propylene rubber (EPR) and termed respectively HPEC1 and HPEC2. Spatial and temporal effects of the aging process were studied by electron spin resonance (ESR) and ESR imaging (ESRI) of HAS-derived nitroxide radicals (HAS-NO), by comparison of thermal transition in original and aged samples using DSC, and by measuring the UV−vis absorption of copolymer films of various thicknesses. The major objectives were to determine the effect of ethylene content (as EPR) and irradiation wavelength on the extent of degradation and to compare with previous ESRI studies of thermal treatment in the same systems.[10] The results presented below reflect predegradation and early degradation stages initiated by UV irradiation and reveal the sensitivity of ESRI methods to early events in the aging process.

Experimental Section

Materials. The two HPEC samples were from Dow Chemical Co.: HPEC1 (IPC C708, $M_n = 60\,700$, $M_w = 227\,000$) and HPEC2 (IPC C104-01, $M_n = 90\,400$, $M_w = 428\,000$). The E content was 25 wt % in HPEC1 and 10 wt % in HPEC2, within a margin of error of ±2%.[10] The HAS (Chart 1) was from Ciba Specialty Chemicals.

Preparation of Samples for ESR and ESRI. HPEC plaques containing 1 wt % Tinuvin 770 and prepared by injection molding were aged by exposure to UVA and UVB

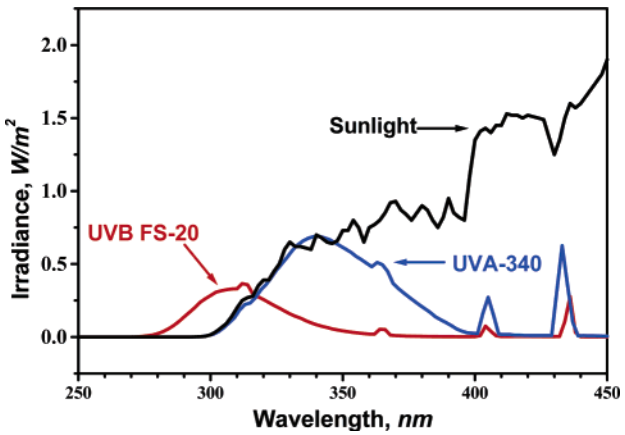

Figure 1. Irradiance as a function of wavelength for UVA-340 and UVB-FS20 fluorescent lamps vs sunlight.

irradiation in UVCON (model UC-327-2) and UV-2 (model MA-24) Atlas weathering chambers, respectively, at 318 K. The UVA source, with half-maximum intensity in the range 320−370 nm, consisted of four UVA340 Sunlamps at 40 W each; the UVB source, with half-maximum intensity in the range 290−330 nm, consisted of four FS-20 Sunlamps at 20 W each. The corresponding irradiances are shown in Figure 1, together with that of sunlight.

For the ESR experiments, cylindrical samples with diameter ≈7 mm were cut through the plaque thickness at selected time intervals, trimmed to fit the 5 mm in diameter of the ESR sample tube, and placed in the ESR resonator with the symmetry axis along the long (vertical) axis of the resonator and parallel to the direction of the magnetic field gradient.

ESR Measurements. Spectra were collected with Bruker X-band EMX spectrometers operating at 9.7 GHz with 100 kHz magnetic field modulation and equipped with the Acquisit 32 Bit WINEPR data system version 3.01 for acquisition and manipulation and ER 4111 VT variable temperature units. The microwave frequency was measured with a Hewlett-Packard 5350B microwave frequency counter. Most spectra were measured with the following parameters: sweep width 120 G, microwave power 2 mW, time constant 40.96 ms, conversion time 81.92 ms, 4−10 scans, and 1024−2048 points. The modulation amplitude was varied in the range 0.5−1.2 G, depending on the line width. The temperature was controlled within ±1 K. All samples were allowed to equilibrate for at least 10 min after reaching the desired temperature. Additional experimental details, including the determination of HAS-NO concentration in whole samples and of the relative intensity of the two nitroxide spectral components, fast (F) and slow (S), have been described.[9,10]

ESR Imaging and Data Acquisition. One of the ESR spectrometers was equipped with two Lewis coils and two regulated dc power supplies for the imaging experiments. The intensity profile of radicals was deduced from 1D ESRI experiments. To this end, two spectra are needed: the usual ESR spectrum and the spectrum measured in the presence of the magnetic field gradient ("1D image"). The 1D image is a convolution of the ESR spectrum in the absence of the gradient with the distribution of the paramagnetic centers along the gradient direction ("the profile"). The deconvolution is correct only if the ESR line shape has no spatial dependence. The two spectra were measured at 340 K in order to reach the motional narrowing regime of both spectral components; in this way the spatial dependence of the ESR signal was avoided. All 1D images were obtained with a field gradient of 200 G/cm.

The intensity profile was fitted by analytical functions and convoluted with the ESR spectrum measured in the absence of the field gradient in order to simulate the 1D image. The genetic algorithm (GA) was used for minimization of the difference between simulated and experimental 1D images; this procedure allowed the best fit to be chosen automatically.[26,27]

The 2D spectral−spatial ESR images were reconstructed from a complete set of projections, typically 128−256, collected as a function of the magnetic field gradient, using a convoluted back-projection algorithm.[9,10] In the first reconstruction stage, the projections at the missing angles were assumed to be identical to the projection measured at the largest available angle. In the second stage, the projections at the missing angles were obtained by the projection slice algorithm (PSA) with 2−10 iterations.[28,29] The 2D image was saved as 128 × 128 or 256 × 256 matrices.

UV−Vis Absorption of HPEC Films. The films were prepared using a Carver compression-molding machine. From the original HPEC ≈3 mm thick plaques, pieces of size 8 × 8 mm^2 were cut and compressed at temperatures in the range 355−393 K and a pressure of 44 atm for 30−180 s. To obtain the thinnest films, the copolymer was compressed directly on the molding stage; for film thicknesses in the range 0.36−1.1 mm, one to four sheets of Teflon frames (thickness 0.140 mm) or a metal frame were used during molding. The film thickness was measured using a Moore and Wright Micro 2000 μm with an accuracy of ≈0.002 mm.

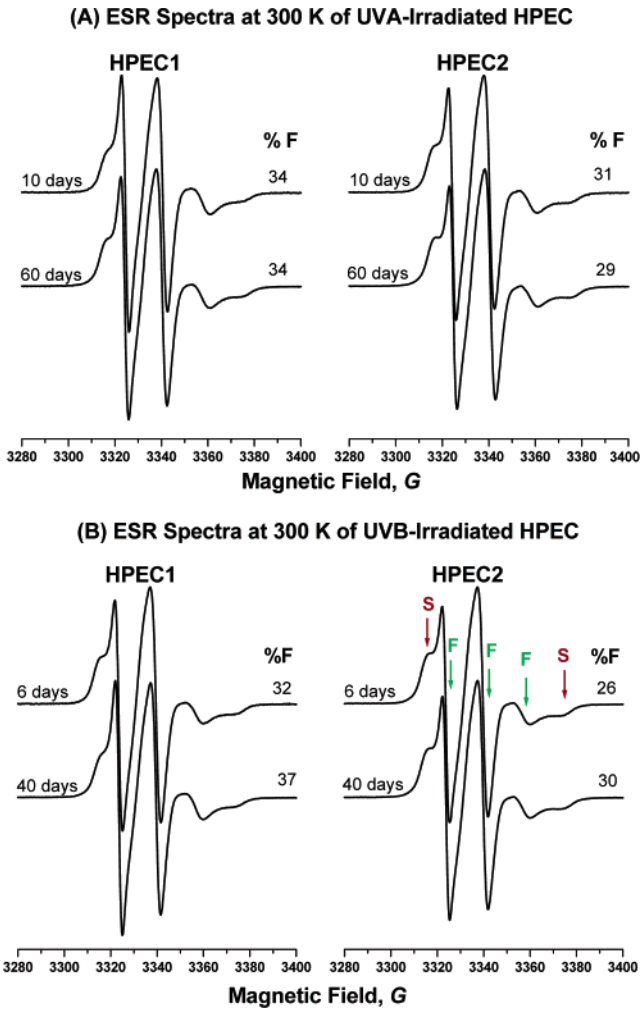

Figure 2. ESR spectra at 300 K in UV-irradiated HPEC1 and HPEC2 (whole samples): (A) UVA, exposure times of 10 and 60 days; (B) UVB, exposure times of 6 and 40 days. Arrows indicate the F and S components. %F is also shown.

Absorbances in the UV−vis range were measured using an Ocean Optics Inc. spectrometer. A blank measurement was taken as a reference before each measurement, and the signal was subtracted from all sample spectra. All measurements were performed at ambient temperature.

DSC Measurements. Thermal transitions were measured at a scan rate of 20 K/min with the TA differential scanning calorimeter model DSC 2920 using the TA Data Analysis Software V4.0.

Results

ESR spectra measured at 300 K in the UVA- and UVB-irradiated HPEC (whole samples) containing 1 wt % HAS are presented in Figure 2. As for the thermally treated copolymers,[10] the spectra consist of two components, fast (F) and slow (S), which reflect the different dynamics of nitroxide radicals in the amorphous phases of the copolymers. The S component represents the rigid amorphous part of EPR and the amorphous part of PP regions, and the F component represents the remaining EPR regions. The relative intensities of the two components are also given in Figure 2. %F is essentially constant with UVA irradiation time and increases slightly with UVB irradiation time.

The concentration of HAS-NO in whole HPEC samples as a function of treatment time t (in days) by the UVB and UVA sources is presented in Figure 3A. The data

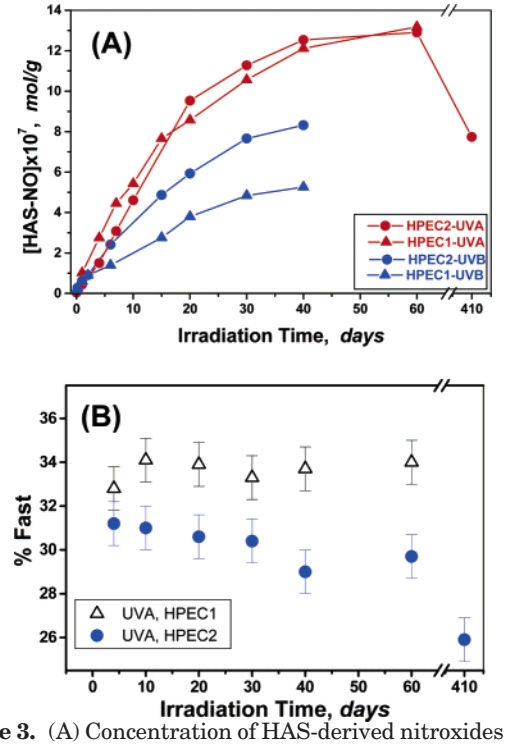

Figure 3. (A) Concentration of HAS-derived nitroxides (HAS-NO) in UV-irradiated HPEC1 and HPEC2. (B) % fast component in the UVA-irradiated samples, both deduced from ESR spectra at 300 K and plotted as a function of irradiation time. Data are for whole samples.

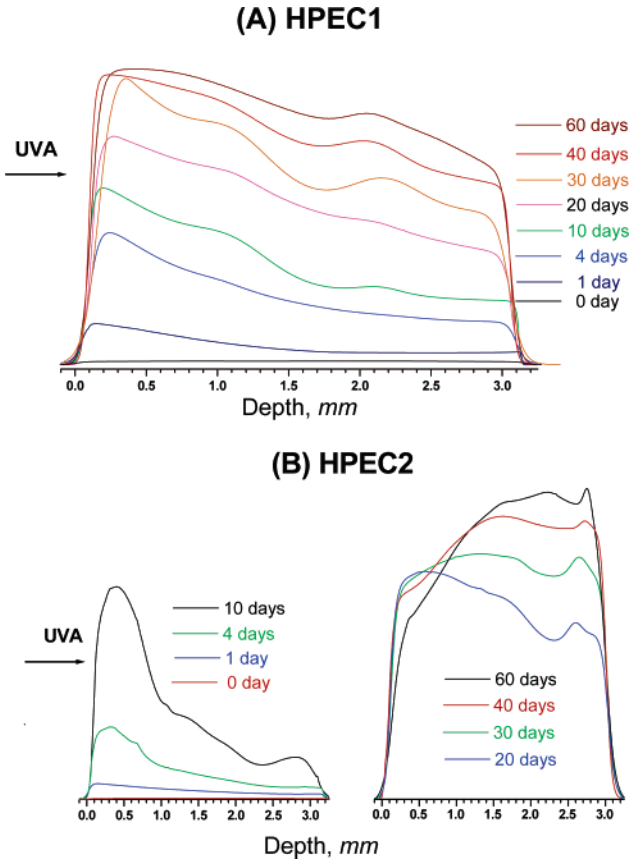

Figure 4. Normalized concentration profiles of HAS-NO in HPEC samples deduced from 1D ESRI, for the indicated UVA irradiation times. (A) HPEC1; (B) HPEC2. Horizontal arrows indicate the irradiated side of the plaque.

points were deduced from corresponding ESR spectra measured at 300 K. For UVA irradiation, the concentration of nitroxides is lower in HPEC2 for $t < 15$ days and slightly higher for $t \geq 15$ days. For UVB irradiation, the concentration of nitroxides is similar in both HPEC samples at short treatment times and higher in HPEC2 for $t \geq 5$ days. The corresponding %F in the UVA-irradiated samples is shown in Figure 3B; considerable change in %F is seen only after the longest treatment time, 410 days, suggesting consumption of the nitroxides in stabilization processes and/or increase of crystallinity due to degradation.

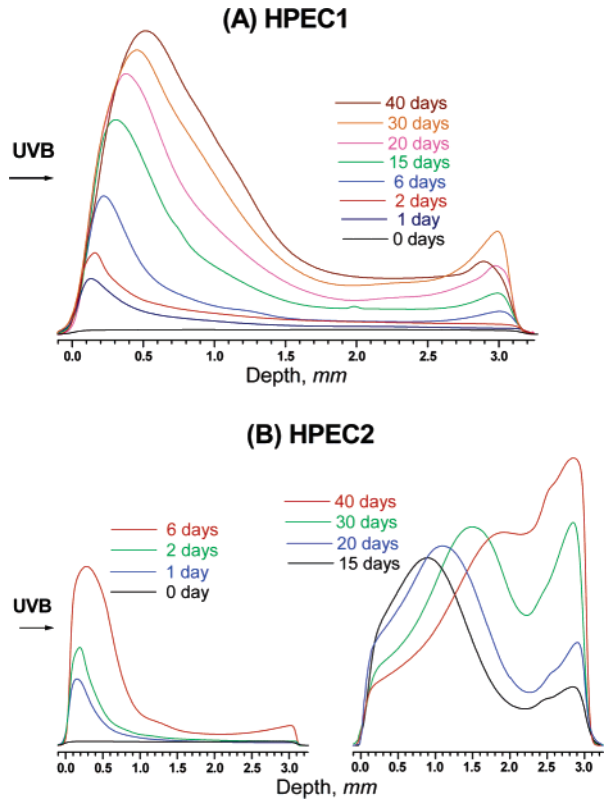

Figure 5. Normalized concentration profiles of HAS-NO in HPEC samples deduced by 1D ESRI, for the indicated UVB irradiation times. (A) HPEC1; (B) HPEC2. Horizontal arrows indicate the irradiated side of the plaque.

The concentration profiles of HAS-NO in HPEC1 and HPEC2 samples that were UVA-irradiated for the indicated t values are shown in parts A and B of Figure 4, respectively. The profiles were normalized according to the total radical concentration in whole samples. The profiles for "0 day" in Figure 4 represent weak nitroxide signals detected even before the UV treatment. For HPEC1, the concentration of HAS-NO increases with treatment time, and the radicals are almost homogeneously distributed within the sample depth (Figure 4A). The nitroxide distribution for HPEC2 is dramatically different: for $t \leq 10$ days, the radicals are concentrated mostly on the irradiated side of the sample, in a layer of thickness $\approx$1 mm; for $t \geq 20$ days, the radical concentration decreases slightly on the irradiated side and nitroxide are present in increasing concentration on the backside.

Figure 5 presents concentration profiles of HAS-NO after UVB irradiation for HPEC1 (Figure 5A) and HPEC2 (Figure 5B). The 1D profiles for both polymers after 1 day of irradiation are similar: radicals are formed on the irradiated side of the sample, in a layer of thickness $<$ 1 mm. In the case of HPEC1, longer treatment times led to additional formation of radicals,

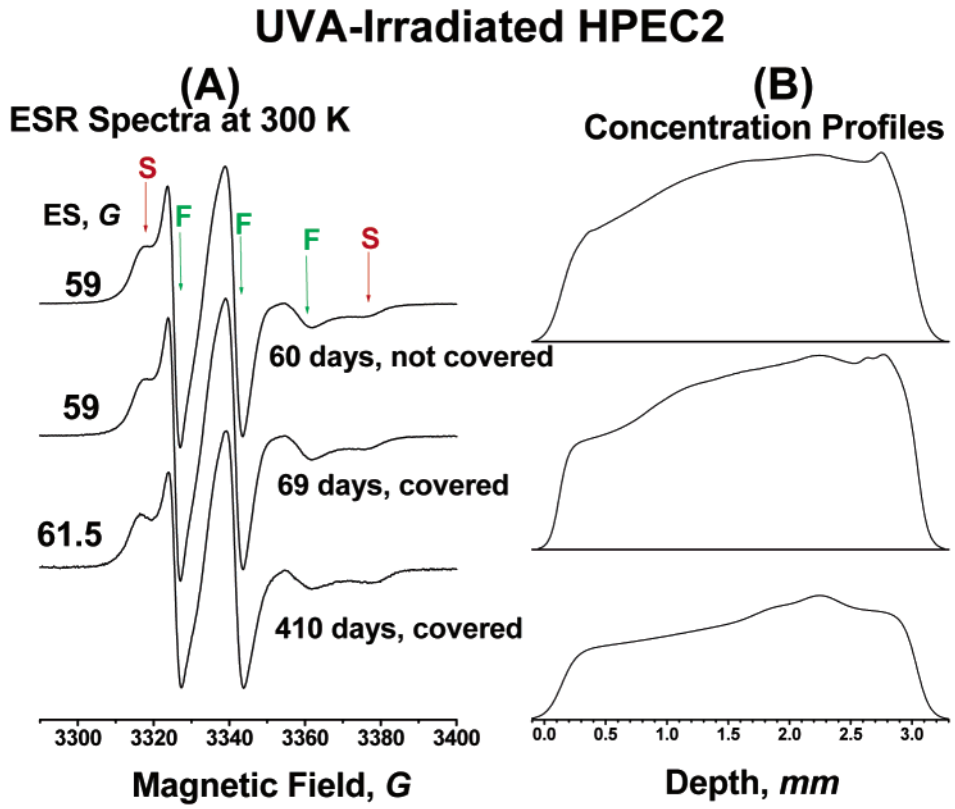

Figure 6. (A) ESR spectra measured at 300 K of HAS-NO radicals in HPEC2 UVA-irradiated for indicated time; ES (*G*) is the extreme separation of the slow (S) component, and F is the fast component. (B) Corresponding normalized concentration profiles deduced by 1D ESRI.

to the displacement of the maximum intensity on the irradiated side into the sample depth, and to a small increase of radical concentration on the backside. For HPEC2, however, the maximum concentration shifts toward the sample center for $t \geq 15$ days, and radicals are formed on the backside; after 40 days of irradiation, the highest radical concentration is observed on the backside of the sample.

No significant differences in ESR spectra and concentration profiles were detected for HPEC2 samples with uncovered and covered (by aluminum foil) backside and irradiated for 60 and 69 days, respectively, as shown in Figure 6; this experiment indicates that nitroxides on the backside are not formed due to scattered light but due to some penetration of UV light through the plaque. The extreme separation of the S component increased to 61.5 G after the largest t (410 days), compared to 59 G for $t = 69$ days; during the same period the concentration profiles did not change noticeably, but the total radical intensity decreases by ≈40% (Figure 6B).

The 2D spectral−spatial ESRI perspective plots for HAS-NO in UVB-irradiated HPEC1 ($t = 20$ days) and UVA-irradiated HPEC2 ($t = 410$ days) are shown in Figure 7, together with "virtual" spectral slices and with corresponding %F values at several distances from the irradiated side. The F/S ratios vary along samples depth. In the case of HPEC1, %F increases from the irradiated side toward the sample interior and is about 2 times higher on the backside compared to the side exposed to light. For HPEC2 after the longest irradiation time ($t = 410$ days), %F is lower on both sides and reaches a maximum in the interior of plaque.

To explain the formation of nitroxides on the back (nonirradiated) side of the plaques, we have measured UV−vis absorptions of polymer films in a range of thicknesses; the results are presented in Figure 8A for HPEC1 and Figure 8B for HPEC2. The corresponding % transmittance at 310 (or 320) and 340 (or 350) nm as a function of film thickness is shown in Figure 9; the wavelengths for comparison were chosen because they represent maxima in the irradiance for UVB and UVA, respectively. For both types of polymers the difference between the transmittances at the two wavelengths is not large but systematic and suggests a lower transmittance for the lower wavelength at all thicknesses, in line with the higher rate of degradation in UVB-irradiated polymers, which will emerge from the Discussion.

Discussion

In this section we will discuss the UV absorption of the copolymers films, assess the effect of irradiation wavelength on the degradation processes, deduce an enhanced degradation rate in the HPEC sample with the lower EPR content (HPEC2), and compare the effect of EPR content on the rate of thermal degradation and photodegradation in the stabilized copolymers.

UV Absorption in HPEC. The specific UV absorption of pure PP is below 200 nm.[30] Any absorption of commercial PP, and also of PE,[31] above this wavelength is due to the presence of impurity chromophores (initiators and catalysts, for example) or additives.

UV absorbances for HPEC films are shown in Figure 8A,B; the peak at 274 nm detected in the thinner HPEC2 films is due to the Organox 1010 UV absorber.[23,32] As seen in Figure 9, for both polymers the amount transmitted is lower in the UVB range (λ = 310−320 nm, at or near the maximum lamp intensity) than in the UVA range (λ = 340−350 nm, at or near

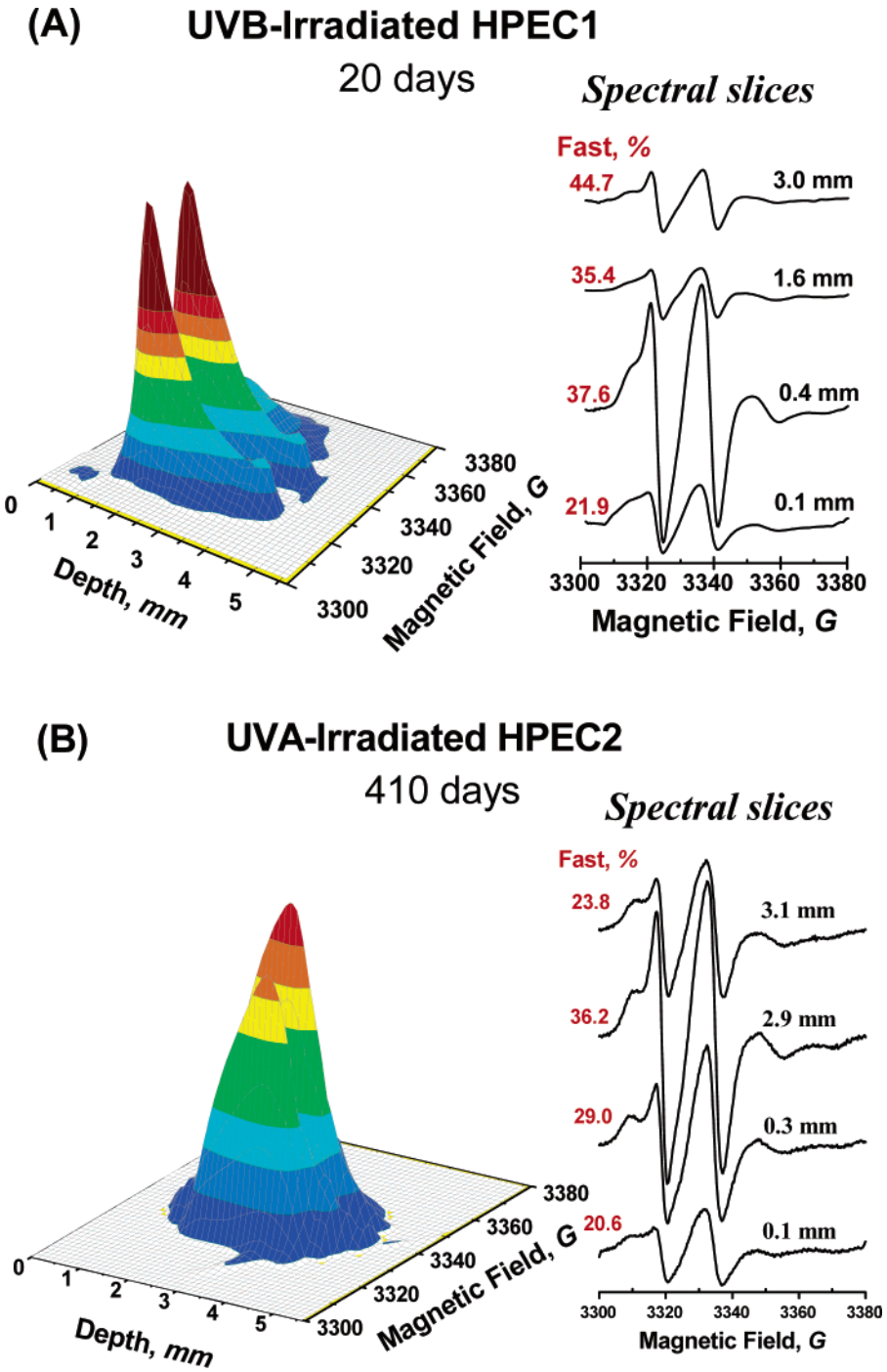

Figure 7. 2D spectral−spatial ESRI perspective image and corresponding virtual slices of HAS-NO radicals in UVB-irradiated HPEC1, $t = 20$ days (A), and in UVA-irradiated HPEC2, $t = 410$ days (B). %F as a function of depth from the irradiated side is also indicated.

the maximum lamp intensity). In addition, the % transmittance for films beyond a thickness of ≈1 mm is small and varies in the range 0.1−0.2%. Three conclusions can be deduced from these observations. (a) The rate of degradation is expected to be higher in samples that were UVB-irradiated; this conclusion is in agreement with the ESRI results (vide infra). (b) Some light penetrates through the plaque thickness and is involved in the formation of nitroxide radicals on the backside of the sample, where oxygen is always present; formation of nitroxides is a facile reaction, and some nitroxides are present even before UV treatment, as seen in Figures 4 and 5 for $t = 0$. Because the intensity of transmitted light is weak, the rate of degradation on the nonirradiated side is negligible, in accord with the concentration profiles shown in Figures 4 and 5; the HAS-NO concentration after long treatment times is high because the nitroxides are not consumed in stabilization processes. (c) Some nitroxides are also formed inside the plaques, as seen clearly in the 1D profiles shown in Figures 4 and in 5B for long treatment times, indicating the presence of oxygen and relatively low degradation rates. These deductions suggest that we are observing low to negligible rates of degradation (with the exception of HPEC2 for $t \geq 20$ days) and set the stage for the discussion that follows.

Effect of Irradiation Wavelength. The HAS-derived nitroxide profile for UVA-irradiated HPEC1

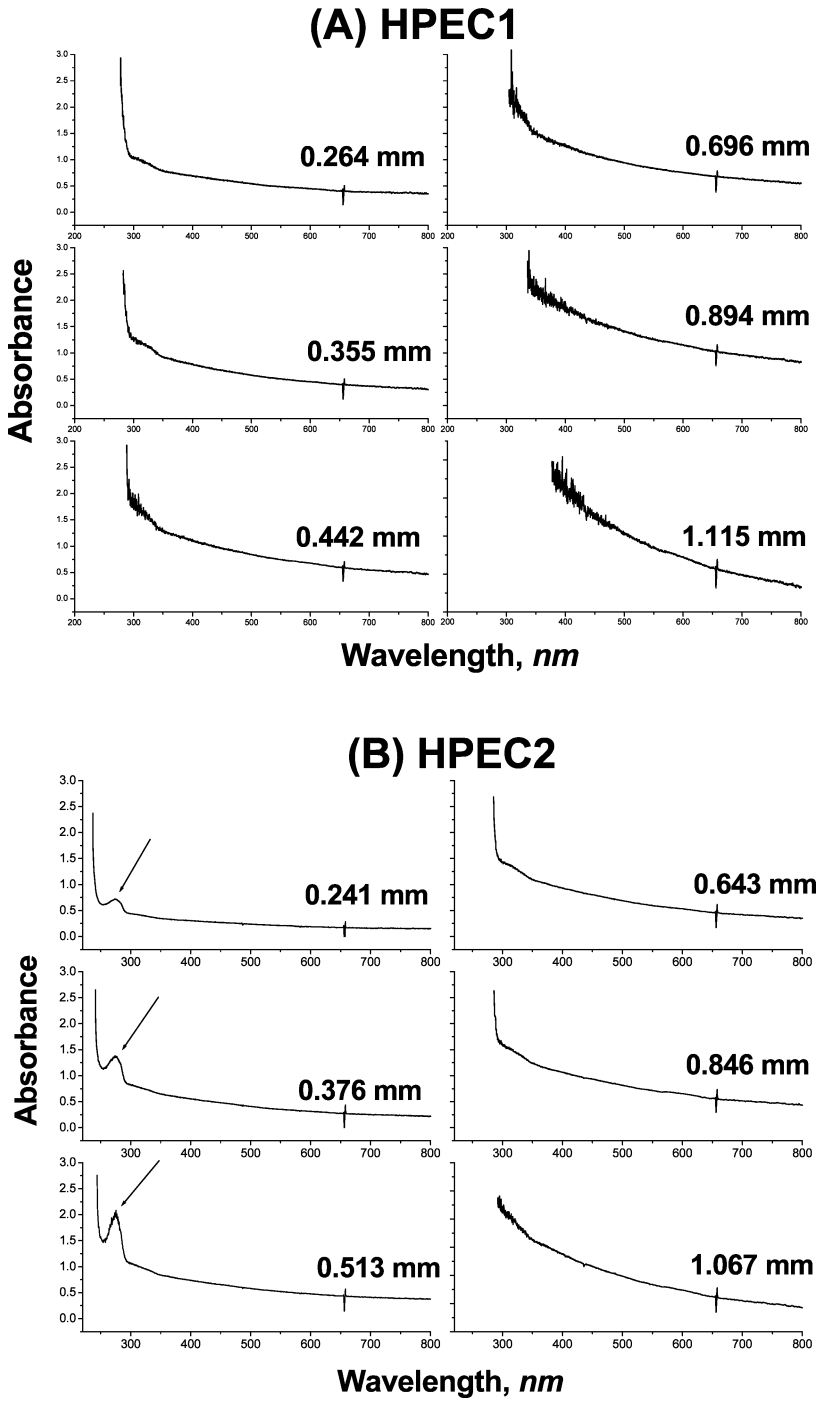

Figure 8. UV−vis absorbances of copolymer films for the indicated film thickness: (A) HPEC1; (B) HPEC2. Arrows in (B) indicate the UV absorption maximum of the antioxidant Organox 1010.

deduced from 1D ESRI (Figure 4A) indicates the presence of nitroxides throughout the sample depth, albeit with a slightly higher concentration on the irradiated side; this result is a sign of a slow degradation rate. Moreover, the %F (Figure 3B) is almost constant with irradiation time: the sample has not reached the DLO regime. The profile for UVB-irradiated HPEC1 (Figure 5A) is dramatically different: spatially heterogeneous degradation is seen both in the low nitroxide concentration for depth ≥ 1.5 mm from the irradiated side and in the displacement of the maximum nitroxide concentration to the sample interior as treatment time increases. Comparison of the profiles for HPEC1 suggests therefore that UVB leads to more advanced degradation, which is limited to a thinner layer compared to UVA. Additional support for this conclusion is obtained by comparison of the profiles for UVA- and UVB-irradiated HPEC2 samples (Figures 4B and 5B, respectively): the profiles for UVB treatment are more heterogeneous, as seen in the presence of nitroxides only in a limited part of the plaque, ≈ 1 mm at the irradiated edge for irradiation time of up to 6 days, and the considerable decrease of radicals concentration on the irradiated side for irradiation time >15 days, an indicator of nitroxide consumption in stabilization steps. This conclusion is reinforced by the variation of %F with sample depth, seen in Figure 7A: %F is low on the irradiated side due to consumption of the F component of the nitroxides in the EPR domains or PP crystallization and very high on the backside, where the rate of degradation is

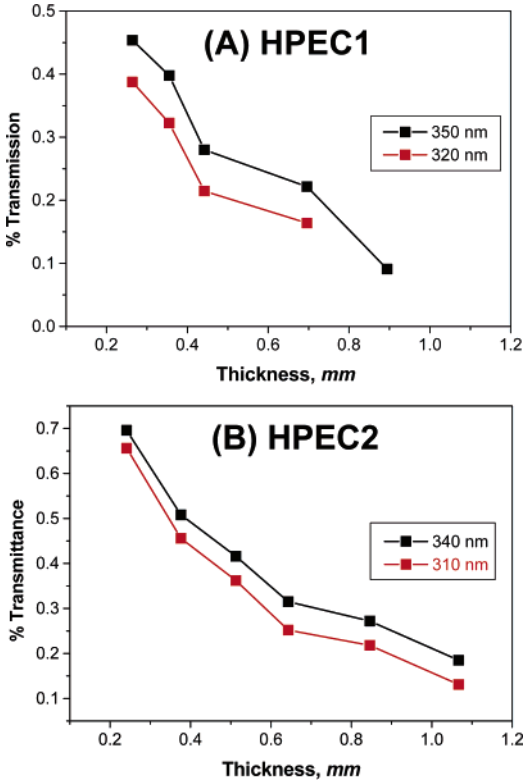

Figure 9. (A) % transmittance at 320 and 350 nm for HPEC1 films. (B) % transmittance at 310 and 340 nm for HPEC2 films, plotted as a function of film thickness.

Table 1. Heats of Transition (ΔH), Melting Temperatures (T_m), and % Crystallinity in HPEC1 and HPEC2 UVA-Irradiated for 60 days[a]

sample[b]	T_m (K)	ΔH (J/g)	% crystallinity
HPEC1 (untreated)	439.0	56.1	26.8
HPEC1-UVA-60 days	439.2	52.8	25.3
HPEC2 (untreated)	439.0	61.6	29.5
HPEC2-UVA-60 days	437.9	75.1	36.0

[a] It was assumed that the heat of transition is 209 J/g for a perfect PP crystal (ref 23). [b] All HPEC samples contained 1 wt % HAS.

negligible. Degradation rates are low, but relatively higher, for the UVB-irradiated samples.

Effect of EPR Content. Clear evidence for the higher degradation rate in HPEC2 compared to HPEC1 is deduced from examination of the nitroxide profiles shown in Figure 4 for UVA-treated samples. The profiles for HPEC1 are almost homogeneous for irradiation times up to and including 60 days. During the same interval the profiles for HPEC2 start as heterogeneous and become complex, with progressively higher distribution of nitroxides within the sample, due to formation of nitroxides that are not consumed in stabilization processes. This conclusion is in accord with the results obtained by Delprat et al., which have suggested that the degradation in the copolymers is essentially driven by the susceptibility of PP to UV degradation.[18]

The DSC data presented in Table 1 add additional support for this conclusion. After 60 days of UVA irradiation, the crystallinity in HPEC1 is similar to the original sample (26.8 and 25.3, essentially the same within experimental error). For HPEC2, however, % crystallinity increases from 29.5 to 36.0% (based on ΔH = 209 J/g[23]), as expected for a higher degradation rate.[22] The lowering of the melting point due to the formation of shorter crystalline segments is only ≈1 K but is similar to that detected in ref 22a for a similar treatment time. The increase of the extreme separation shown in Figure 6 to 61.5 G upon the longest treatment time with UVA, 410 days, also indicates a higher degree of crystallinity: the slow (S) component becomes more rigid due to its proximity to crystalline domains (the "rigid amorphous phase").[10a]

In explaining the decrease of the melting point with increasing irradiation time, Rabello and White also considered the possible degradation at the lamellar fold surfaces, which can result in a reduction of the melting temperature due to the increase in the surface free energy of the crystals.[22a] This possibility is, however, contrary to the result that PP samples with higher crystallinity "displayed less degradation"[22] and therefore not realistic.

UV vs Thermal Aging. In the study of thermal degradation of HPEC systems, we have deduced by both ESRI and FTIR that the rate of degradation is higher in HPEC1, which contains the higher (25 wt %) E content.[10b] This result was explained by the higher diffusion rate of oxygen and reactant mobility at the aging temperatures (393 and 433 K) in copolymers that contained *more* E. The higher degradation rate deduced in the present study for UV-irradiated HPEC that contained *less* E (HPEC2) indicates a different behavior in thermally treated and UV-irradiated copolymers. Delprat and Gardette suggested that thermal degradation and photodegradation give rise to similar products, due in both cases to the susceptibility of PP to oxidation.[18] We agree that the dominant effect in degradation is the PP sensitivity at the point of attack, the tertiary carbon. However, even if in both types of treatment PP is the major component that undergoes oxidation, the rate of degradation is sensitive to the amount of EPR, which influences the rate of oxygen diffusion. This deduction was possible in this study, which compared two HPEC compositions differing in EPR content. Moreover, a different oxidation mechanism for PP undergoing thermal oxidation and photooxidation has been reported in recent papers, using $^{32}O_2$ and $^{36}O_2$:[21] only photodegradation led to the formation of $^{34}O_2$. To explain this result, two reactions involving peroxy radicals ROO$^\bullet$ have been considered; the first is H abstraction from the polymer PH, and the second is peroxy radicals recombination and dissociation:

$$ROO^\bullet + PH \rightarrow ROOH \text{ and } P^\bullet \quad (1)$$

$$2ROO^\bullet \rightarrow 2RO^\bullet + O_2 \quad (2)$$

The first reaction is favored at higher temperatures, because of the higher activation energy, and is expected upon thermal treatment. The second reaction has a lower activation energy, can take place at lower temperatures, and leads to the formation of $^{34}O_2$. The different behavior of PP at different temperatures is expected to be carried over to HPEC systems as well.

Conclusions

Analysis of the results has led to the following major conclusions: (1) Small intensity of UV light transmitted through the plaque thickness is sufficient for the formation of HAS-derived nitroxides on the nonirradiated side, where the radical concentration is high because nitroxides are not consumed in stabilization processes,

and the rate of degradation is negligible. (2) UV irradiation leads to degradation only on the irradiated side, and the nitroxides are consumed in the stabilization process. This effect is more pronounced for UVB-irradiated samples. (3) HPEC2 (10% E) degrades faster compared to HPEC1 (25% E); this result is in contrast to the behavior of thermally treated HPEC samples.

Acknowledgment. This study was supported by the Polymers Program of the National Science Foundation. We are grateful to Rose Ryntz and Ewa Lebert (Visteon) for their help with the DSC measurements and to Dow and Ciba Co. for the gift of HPEC and HAS, respectively. Special thanks go to John L. Gerlock for useful discussions and suggestions and for his help with plaque preparation. We are grateful to one reviewer for his/her careful reading of the manuscript and for helpful and constructive criticism.

References and Notes

(1) Ohno, K. In *EPR Imaging and In Vivo EPR*; Eaton, S. S., Eaton, G. R., Ohno, K., Eds.; CRC Press: Boca Raton, FL, 1991; Chapter 18, p 181.
(2) Scott, G. In *Atmospheric Oxidation and Antioxidants*; Scott, G., Ed.; Elsevier: Amsterdam, 1993; Vol. II, Chapter 5, p 279.
(3) Pospisil, J. *Adv. Polym. Sci.* **1995**, *124*, 87.
(4) (a) Lucarini, M.; Pedulli, G. F.; Borzatta, V.; Lelli, N. *Res. Chem. Intermed.* **1996**, *22*, 581. (b) Lucarini, M.; Pedulli, G. F. *Angew. Makromol. Chem.* **1997**, *252*, 179. (c) Franchi, P.; Lucarini, M.; Pedulli, G. F.; Bonora, M.; Vitali, M. *Macromol. Chem. Phys.* **2001**, *202*, 1246.
(5) Lucarini, M.; Pedulli, G. F.; Motyakin, M. V.; Schlick, S. *Prog. Polym. Sci.* **2003**, *28*, 331−340.
(6) Billingham, N. C. In *Atmospheric Oxidation and Antioxidants*; Scott, G., Ed.; Elsevier: Amsterdam, 1993; Vol. II, Chapter 4, p 219.
(7) (a) Gillen, K. T.; Clough, R. L.; Dhooge, N. J. *Polymer* **1986**, *27*, 225. (b) Gillen, K. T.; Clough, R. L.; Quintana, C. A. *Polym. Degrad. Stab.* **1987,** *17*, 31.
(8) Gillen, K. T.; Clough, R. L.; Wise, J. In *Polymer Durability: Degradation, Stabilization and Lifetime Prediction*; Clough, R. G., Billingham, N. C., Gillen K. T., Eds.; Adv. Chem. Ser. 249; American Chemical Society: Washington, DC, 1996; Chapter 34, p 557.
(9) (a) Motyakin, M. V.; Gerlock, J. L.; Schlick, S. *Macromolecules* **1999**, *32*, 5463. (b) Kruczala, K.; Motyakin, M. V.; Schlick, S. *J. Phys. Chem. B* **2000**, *104*, 3387. (c) Motyakin, M. V.; Schlick, S. *Macromolecules* **2001**, *34*, 2854. (d) Motyakin, M. V.; Schlick, S. *Polym. Degrad. Stab.* **2002**, *76*, 25. (e) Motyakin, M. V.; Schlick, S. *Macromolecules* **2002**, *35*, 3984. (f) Motyakin, M. V.; Schlick, S. *Polym. Degrad. Stab.*, in press.
(10) (a) Kruczala, K.; Varghese, B.; Bokria, J. G.; Schlick, S. *Macromolecules* **2003**, *36,* 1899. (b) Kruczala, K.; Bokria, J. G.; Schlick, S. *Macromolecules* **2003**, *36,* 1909.
(11) Bokria, J. G.; Schlick, S. *Polymer* **2002**, *43*, 3239.
(12) (a) Varghese, B.; Schlick, S. *J. Polym. Sci., Part B: Polym. Phys.* **2002**, *40*, 415. (b) Varghese, B.; Schlick, S. *J. Polym. Sci., Part B: Polym. Phys*. **2002**, *40*, 424.
(13) Albizzati, E.; Giannini, U.; Collina, G.; Noristi, L.; Resconi, L. In *Polypropylene Handbook*; Moore, E. P., Jr., Ed.; Hanser Publishers: Munich, 1996; Chapter 2, p 92.
(14) Flory, P. J. *J. Phys. Chem.* **1949**, *17*, 233.
(15) Cheng, S. Z. D.; Wunderlich, B. *Macromolecules* **1988**, *21*, 789.
(16) Wunderlich, B. *Thermal Analysis;* Academic Press: Boston, 1990. (b) *Prog. Polym. Sci.* **2003**, *28*, 383.
(17) Mandelkern, L. *Acc. Chem. Res.* **1990**, *23*, 380.
(18) Delprat, P.; Duteurtre, X.; Gardette, J.-L. *Polym. Degrad. Stab.* **1995**, *50*, 1.
(19) HALS-1 was identified as Tinuvin 770, which was also used in our experiments. HALS-2 was not identified but was probably a stabilizer with a higher molecular mass.
(20) Rånby, B.; Rabek, J. F. *Photo-degradation, Photo-oxidation and Photostabilization of Polymers*; Wiley: New York, 1975; Chapter 4, pp 120−141.
(21) (a) Philippart, J.-L.; Gardette, J.-L. *Polym. Degrad. Stab.* **2001**, *71*, 189. (b) Philippart, J.-L.; Gardette, J.-L. *Polym. Degrad. Stab*. **2001**, *73*, 185.
(22) (a) Rabello, M. S.; White, R. J. *Polym. Degrad. Stab.* **1997**, *56*, 55. (b) Rabello, M. S.; White, R. J. *Polymer* **1997**, *38*, 6379, 6389. (c) Shyichuk, A. V.; Stavychna, D. Y.; White, R. J. *Polym. Degrad. Stab.* **2001**, *72*, 279.
(23) (a) Milosavljevic, B. H.; Novakovic, Lj. *Nucl. Instrum. Methods Phys. Res. B* **1999**, *151*, 462.
(24) Kotek, J.; Kelnar, I.; Baldrian, J.; Raab, M. *Eur. Polym. J.* **2004**, *40*, 2731.
(25) (a) Mirabella, F. M. *Polymer* **1993**, *34*, 1729. (b) Mirabella, F. M. *J. Polym. Sci., Part B: Polym. Phys.* **1994**, *32*, 1205. (c) Mirabella, F. M., Jr.; McFaddin, D. C. *Polymer* **1996**, *37*, 931.
(26) (a) Goldberg, D. E. *Genetic Algorithms in Search, Optimization and Machine Learning.* Addison-Wesley: Reading, 1989. (b) Michalewicz, Z. *Genetic Algorithms + Data Structures = Evolution Programs*; Springer-Verlag: Berlin, 1992.
(27) Spalek, T.; Kruczala, K.; Sojka, Z.; Schlick, S., manuscript in preparation.
(28) Maltempo, M. M.; Eaton, S. S.; Eaton, G. R. In *EPR Imaging and In Vivo EPR*; Eaton S. S., Eaton, G. R., Ohno, K., Eds.; CRC Press: Boca Raton, FL, 1991; Chapter 14, p 145.
(29) Marek, A.; Schlick, S., unpublished work from this laboratory. See also refs 9c−f and 10b.
(30) Partridge, R. H. *J. Chem. Phys.* **1968**, *49*, 3656, and references therein.
(31) The UV absorption of PE commences ≈30 nm below that for PP.
(32) Morlat, S.; Mailhot, B.; Gonzalez, D.; Gardette, J.-L. *Chem. Mater.* **2004**, *16*, 377.

MA0502194